Environmental Science & Technology

Article

pubs.acs.org/est

$[MoS_4]^{2-}$ Cluster Bridges in Co−Fe Layered Double Hydroxides for Mercury Uptake from S−Hg Mixed Flue Gas

Haomiao Xu,[†,‡] Yong Yuan,[†] Yong Liao,[†] Jiangkun Xie,[†] Zan Qu,[†] Wenfeng Shangguan,[‡] and Naiqiang Yan*[,†]

[†]School of Environmental Science and Engineering, Shanghai Jiao Tong University, 800 Dongchuan Road, Minhang District, Shanghai 200240, China

[‡]Research Center for Combustion and Environment Technology, Shanghai Jiao Tong University, Shanghai 200240, China

Supporting Information

ABSTRACT: $[MoS_4]^{2-}$ clusters were bridged between CoFe layered double hydroxide (LDH) layers using the ion-exchange method. $[MoS_4]^{2-}$/CoFe-LDH showed excellent Hg^0 removal performance under low and high concentrations of SO_2, highlighting the potential for such material in S−Hg mixed flue gas purification. The maximum mercury capacity was as high as 16.39 mg/g. The structure and physical-chemical properties of $[MoS_4]^{2-}$/CoFe-LDH composites were characterized with FT-IR, XRD, TEM&SEM, XPS, and H_2-TPR. $[MoS_4]^{2-}$ clusters intercalated into the CoFe-LDH layered sheets; then, we enlarged the layer-to-layer spacing (from 0.622 to 0.880 nm) and enlarged the surface area (from 41.4 m^2/g to 112.1 m^2/g) of the composite. During the adsorption process, the interlayer $[MoS_4]^{2-}$ cluster was the primary active site for mercury uptake. The adsorbed mercury existed as HgS on the material surface. The absence of active oxygen results in a composite with high sulfur resistance. Due to its high efficiency and SO_2 resistance, $[MoS_4]^{2-}$/CoFe-LDH is a promising adsorbent for mercury uptake from S−Hg mixed flue gas.

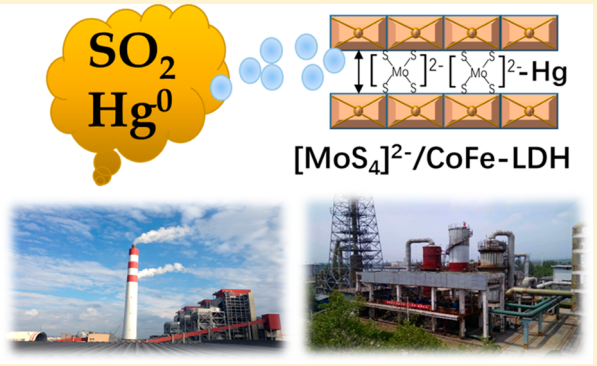

INTRODUCTION

Mercury is a highly toxic pollutant, discharging from industries into the atmosphere and causing severe harmful environmental pollution.[1−3] Mercury often stably exists in coal and industrial ore and is present as HgS. However, after high-temperature combustion from the above-mentioned industrial production process,[4,5] stable mercury is stripped from the raw materials and exists as gaseous elemental mercury (Hg^0) in high-temperature flue gas. Meanwhile, stable sulfur is also released after thermal decomposition processes and primarily exists as SO_2 in the flue gas, resulting in S−Hg mixed flue gas. In addition, S−Hg mixed flue gases often exist in many types of flue gases, especially in nonferrous plants.[6,7] High concentrations of gaseous mercury and SO_2 coexist in smelting gas. The mixed gas is difficult to control using traditional mercury control technologies.

Many technologies have been developed to remove Hg^0 from S−Hg mixed flue gases. In general, catalytic oxidation and adsorption methods have often been used to stabilize mercury in liquid and solid materials.[4,5] The catalytic oxidation method converts gaseous Hg^0 to an oxidized state (Hg^{2+}, such as $HgCl_2$, $HgBr_2$, and HgO). The oxidized mercury can be adsorbed by fly ash or slurry. The adsorption method changes gaseous Hg^0 or Hg^{2+} to its particle-bound state (Hg^p). Various materials, such as activated carbon, fly ash, noble metals, and transition-metal oxides, have been employed for the adsorption of metal ions.[4,5,8] Carbon-based materials, such as active carbon and fly ash, have mercury holding capacity due to the abundant porous structure.[9] To enhance the mercury capacity, some chemicals that have high affinity performance, such as halogens,[10] sulfur,[8,11] and transition-metal oxides,[12] have been used to modify carbon-based sorbents. Transition-metal oxides, such as MnOx[13,14] and FeOx,[15] have high catalytic oxidation and adsorption performances for gaseous mercury. After modification, Ce-MnOx and Fe-TiOx binary metal oxides often have large mercury capacities. However, these selected catalysts or sorbents are often poisoned due to the presence of SO_2.[16−18] Surface oxygen is the primary binding site for mercury.[19] SO_2 can cause surface sulfation and occupy surface oxygen sites, resulting in low activity for Hg^0 from S−Hg mixed flue gas. The mercury binding sites are occupied by SO_4^{2-}. In this process, SO_2 is oxidized to SO_3 by transition-metal oxides and reacted with surface oxygen to form SO_4^{2-}, resulting in low mercury capacity.

Sulfur is one element with affinity for mercury, and HgS stably exists in ore. Sulfur is often used as a sorbent for chemical stabilization when capturing Hg^0. However, the

Received: June 13, 2017
Revised: July 25, 2017
Accepted: July 27, 2017
Published: July 31, 2017

DOI: 10.1021/acs.est.7b02537
Environ. Sci. Technol. 2017, 51, 10109−10116

reaction between solid S and gaseous Hg^0 is slow. Chalcogenides can accelerate this reaction. Li et al. found that nano-ZnS with a high surface area has a high mercury capacity and that mercury primarily exists as HgS on the material's surface.[20] Yang et al. selected magnetic pyrrhotite, derived from the thermal treatment of natural pyrite, to remove and recover Hg^0 from flue gas. It has a fast reaction rate and a high mercury adsorption capacity.[21] Recent studies have found that polysulfides are efficient mercury sorbents for Hg^{2+} or Hg^0 capture. Transition-metal complexes, such as $CoMoS/\gamma\text{-}Al_2O_3$, were prepared as a sorbent for Hg^0 capture.[22] Chalcogels showed promising catalytic and gas separation performances. Some polysulfide chalcogels with ion-exchange properties participated in vapor sorption.[23] The ion-exchangeable molybdenum sulfide chalcogel exhibited high adsorption selectivities for CO_2 and C_2H_6 over H_2 and CH_4. This aerogel was also useful for capturing iodine and mercury.[24]

However, the main challenge could be that polysulfide should be supported by a suitable material. Layered double hydroxides (LDHs), which are composed of mixed metal oxides with the chemical formula $[M^{2+}_{1-x}M^{3+}_x(OH)_2]^{x+}[(A^{n-})_{x/n}]^{x-}\cdot mH_2O$, have excellent intercalation and ion-exchange properties.[25−27] Such structure is beneficial for building a bridge structure. Previous studies have reported that polysulfide $[S_x]^{2-}$ (x = 2, 4) species were intercalated into a Mg−Al layered double hydroxide (MgAl-LDH) by a $[S_x]^{2-}/NO^{3-}$ anion-exchange reaction. S_x-MgAl-LDH materials exhibit excellent performances for Cu^{2+}, Ag^+, and Hg^{2+} ion removal.[25] In addition, S_x/MgAl-LDH (x = 2, 4, 5) can efficiently capture large quantities of mercury (Hg^0) vapor.[28] The $[MoS_4]^{2-}$ cluster ions were intercalated into MgAl-NO_3-LDH to produce MgAl-MoS_4-LDH, which demonstrates highly selective binding and extremely efficient removal of heavy metal ions, such as Cu^{2+}, Pb^{2+}, Ag^+, and Hg^{2+}.[29] One advantage is that this type of structure resulted in a porous material that was beneficial for gas transfer and surface reaction. Another advantage is that the O binding atoms were removed using anion-exchange methods. Sulfur clusters replaced O in the bridge. This could be useful when SO_2 is present in the simulated gases.

In this study, we report a series of $[MoS_4]^{2-}$ cluster-modified LDH materials for removing Hg^0 from simulated flue gas. CoFe-NO_3^--LDH, NiAl-NO_3^--LDH, ZnAl-NO_3^--LDH, and CoAl-NO_3^--LDH were prepared as the supports for $[MoS_4]^{2-}$ clusters. The Hg^0 removal performances over these composites were evaluated in a fixed-bed adsorption system. The mechanism for Hg^0 removal was discussed based on the characterization results.

EXPERIMENTAL SECTION

Preparation of Materials. *Synthesis of NO_3^--LDH Materials.* In a typical procedure, nitrate salts of the metals were selected to prepared LDH materials. To synthesize CoFe-NO_3^--LDH, 20 mmol of $Co(NO_3)_2$ and 10 mmol of $Fe(NO_3)_2$ were dissolved in 100 mL of deionized water and stirred for 1 h. Afterward, NaOH solution was used to adjust the pH to 10. The product was then filtered, washed with deionized water, and air-dried at 80 °C. Similarly, NiAl-NO_3^--LDH, ZnAl-NO_3^--LDH, and CoAl-NO_3^--LDH were prepared by the same method. The ratios of Ni:Al, Zn:Al, and Co:Al were 2:1.

Synthesis of $[MoS_4]^{2-}$/LDH Materials. $[MoS_4]^{2-}$/LDH was prepared via an anion-exchange reaction. For $[MoS_4]^{2-}$/CoFe-LDH, briefly, 0.4 g of as-prepared CoFe-NO_3^--LDH was dissolved in deionized water under ultrasonic treatment for 30 min. Then, 0.4 g of $(NH_4)_2MoS_4$ powder was dissolved in deionized water. The two solutions were mixed together with stirring at ambient temperature for 24 h. The resulting products were filtered and washed with deionized water. Finally, the samples were air-dried at 80 °C. The $[MoS_4]^{2-}$/NiAl-LDH, $[MoS_4]^{2-}$/ZnAl-LDH, and $[MoS_4]^{2-}$/CoAl-LDH were prepared using the same method. For comparison, S_4/CoFe-LDH was also synthesized. Then, 1 mmol of Na_2S and 3 mmol of elemental sulfur were mixed together and stirred at 90 °C until the sulfur absolutely dissolved. The mixed solution was added to the CoFe-NO_3^--LDH solution with 0.4 g of CoFe-LDH. The product was also filtered, washed with deionized water, and air-dried at 80 °C.

Characterization of Materials. X-ray diffraction (XRD) patterns were obtained using a Shimadzu XRD-6100 diffractometer with Cu−Kα radiation. The data were recorded at a scan rate of 10 deg·min^{-1} in the 2θ range from 10 to 80°. FT-IR spectroscopy was performed to characterize the surface properties. The H_2-TPR experiments were performed on a Chemisorp TPx 290 instrument. The samples were degassed at 200 °C for 3 h under an Ar atmosphere before the tests, and the reducing gas was 10% H_2/Ar. X-ray photoelectron spectroscopy (XPS) results were recorded with an Ultra DLD (Shimadzu−Kratos) spectrometer with Al Kα as the excitation source, and the C 1s line at 284.6 eV was used as a reference for the binding energy calibration. The microstructures of the materials were characterized by field emission scanning electron microscopy (SEM, JSM-7001F) and transmission electron microscopy (TEM, JEM-2100, operating at 200 kV). The BET (Brunauer−Emmett−Teller) surface areas of the samples were determined using N_2 adsorption at −196 °C using a quartz tube (Quantachrome 2200e).

Measurement of Gaseous Mercury Adsorption Performances. A lab-scale fixed-bed adsorption system was assembled to evaluate the Hg^0 removal efficiency by the as-prepared materials, as shown in the Supporting Information (Figure S1). The system contains the gas distributing system, reaction system, Hg^0 detection system, and tail gas purification system. In general, O_2 and SO_2 vapor was prepared with pure N_2. The fixed-bed reactor was constructed to allow for a total gas flow of 500 mL/min at temperatures from 50 to 150 °C. Then, 20 mg of prepared material was used for each experiment, and it was placed in a quartz tube with a diameter of 4 cm. In addition, active carbon and $KMnO_4$ solution were used for the off-gas cleaning. Active carbon can adsorb the mercury (Hg^{2+} and Hg^0) in the flue gas. $KMnO_4$ was used for adsorbing the oxidized mercury.

In each test, the mercury inlet gas bypassed the sorbent bed and passed into the analytical system until the desired inlet mercury concentration was established. A cold vapor atomic absorption spectrometer mercury detector (CVASS) was used to detect the concentration of off-gas, which was calibrated by Lumex RA 915+. Temperature control devices were installed to control the mixed gas and reactor temperature. To investigate the effect of temperature on the flue gas, the area under the breakthrough curves, corresponding to Hg^0 on the prepared sorbents during 180 min, was integrated. To investigate the effects of various gas components, various SO_2 concentrations were chosen when needed. The Hg^0 removal efficiency and mercury adsorption capacity were calculated according to eqs 1 and 2

DOI: 10.1021/acs.est.7b02537
Environ. Sci. Technol. 2017, 51, 10109−10116

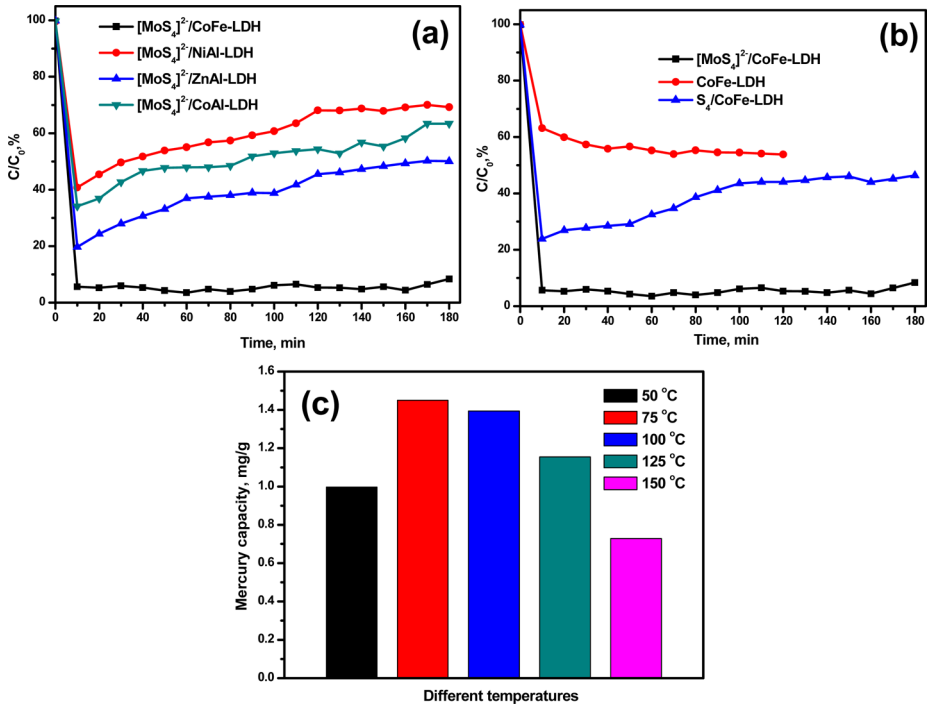

Figure 1. Performances of gaseous mercury removal performances (a) over various $[MoS_4]^{2-}$ intercalated LDH materials (75 °C); (b) CoFe-LDH, S_4/CoFe-LDH, and $[MoS_4]^{2-}$/CoFe-LDH materials (75 °C), and (c) under different temperatures over $[MoS_4]^{2-}$/CoFe-LDH materials (50−125 °C) Reaction conditions: 4% O_2 and 350 $\mu g/m^3$ Hg0 with 500 mL/min flow rate.

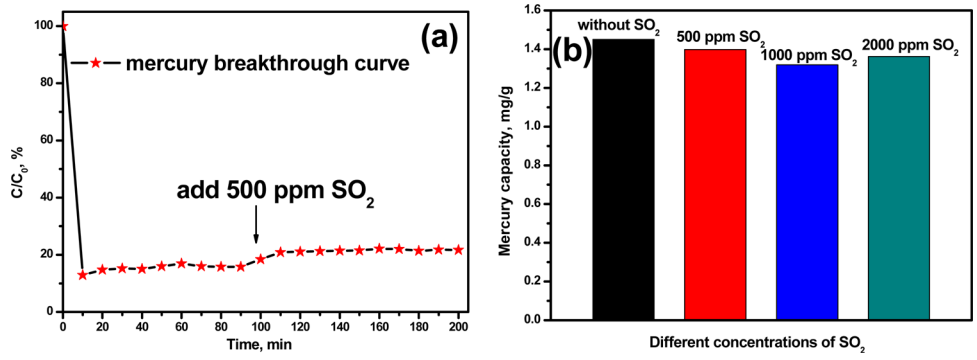

Figure 2. Effects of SO_2 on Hg^0 removal over $[MoS_4]^{2-}$/CoFe-LDH material, (a) mercury breakthrough curve when 500 ppm of SO_2 was added to the simulated flue gas and (b) under different concentrations of SO_2. Reaction conditions: 4% O_2 and 350 $\mu g/m^3$ Hg0 with 500 mL/min flow rate.

$$\text{removal efficiency} = \frac{Hg^0_{in} - Hg^0_{out}}{Hg^0_{in}} \times 100\% \quad (1)$$

$$Q = \frac{1}{m}\int_{t_2}^{t_1} (Hg^0_{in} - Hg^0_{out}) \times f \times dt \quad (2)$$

where the Hg^0_{in} is the inlet concentration of Hg^0, and Hg^0_{out} is the outlet concentration of Hg^0. Q is the Hg^0 adsorption capacity, m is the mass of the sorbent in the fixed-bed, f denotes the flow rate of the influent, and t_1 and t_2 represent the initial and ending test times of the breakthrough curves.

RESULTS AND DISCUSSION

Elemental Mercury Removal Performances. The performances of as-prepared $[MoS_4]^{2-}$ clusters that modified various LDH materials were evaluated in a fixed-bed adsorption system. As shown in Figure 1(a), $[MoS_4]^{2-}$ clusters that intercalated CoFe-LDH, NiAl-LDH, ZnAl-LDH, and CoAl-LDH materials were selected for Hg^0 removal at 75 °C with 4% O_2. These composites exhibited different performances. $[MoS_4]^{2-}$/NiAl-LDH had the lowest activity among the as-prepared samples, after 180 min of reaction, and it only had approximately 31% Hg^0 removal efficiency. $[MoS_4]^{2-}$/CoAl-LDH and $[MoS_4]^{2-}$/ZnAl-LDH materials enhanced the removal performances compared with $[MoS_4]^{2-}$/NiAl-LDH, with removal efficiencies of 39% and 50%, respectively. $[MoS_4]^{2-}$/CoFe-LDH had the highest Hg^0 removal efficiency among these prepared materials. It had greater than 90% Hg^0 removal efficiency even after 180 min of reaction. The reaction activities of the four as-prepared kinds of $[MoS_4]^{2-}$ clusters modified LDH materials follow the order of $[MoS_4]^{2-}$/CoFe-LDH > $[MoS_4]^{2-}$/ZnAl-LDH > $[MoS_4]^{2-}$/CoAl-LDH > $[MoS_4]^{2-}$/NiAl-LDH.

Furthermore, the Hg^0 removal performances of CoFe-LDH and $[S_4]^{2-}$/LDH were evaluated for comparison. As shown in Figure 1(b), CoFe-LDH had approximately 50% Hg^0 removal efficiency. With the modification of poly sulfur, S_4/CoFe-LDH

DOI: 10.1021/acs.est.7b02537
Environ. Sci. Technol. 2017, 51, 10109−10116

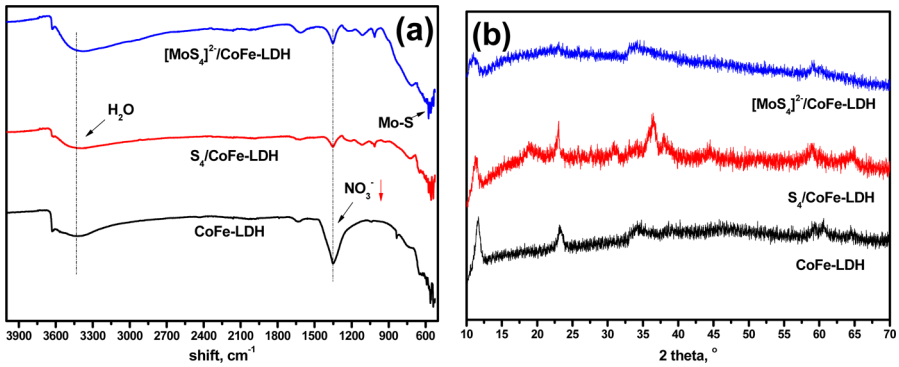

Figure 3. (a) FT-IR spectra and (b) XRD patterns of CoFe-LDH, S_4/CoFe-LDH, and $[MoS_4]^{2-}$/CoFe-LDH material.

increased the Hg^0 removal efficiency by approximately 10%. However, it was still lower than that of $[MoS_4]^{2-}$/CoFe-LDH. Obviously, after $[MoS_4]^{2-}$ cluster modification, the Hg^0 removal performance was significantly improved. The results indicated that $[MoS_4]^{2-}$ clusters may have a better mercury capture capacity than S_4 poly sulfur.

Figure 1(c) gives the mercury adsorption capacity for 180 min under various temperatures over $[MoS_4]^{2-}$/CoFe-LDH. When the temperature was 50 °C, the mercury capacity was 0.99 mg/g for 180 min of reaction. When the temperature increased to 75 °C, it had the highest mercury capacity of 1.45 mg/g. However, the Hg^0 removal efficiencies and mercury capacities decreased when the temperature continued to increase. $[MoS_4]^{2-}$/CoFe-LDH had mercury capacities of 1.39 and 1.15 mg/g at 100 and 125 °C, respectively. In addition, a higher temperature could result in deactivity for Hg^0. $[MoS_4]^{2-}$/CoFe-LDH only had a mercury capacity of 0.73 mg/g at 150 °C. A higher temperature was not favorable for Hg^0 uptake over $[MoS_4]^{2-}$/CoFe-LDH. The mercury adsorption breakthrough curve over the $[MoS_4]^{2-}$/CoFe-LDH composite was evaluated (shown in Figure S2), and the mercury adsorption capacity was as high as 16.39 mg/g.

The effect of SO_2 on Hg^0 removal was evaluated, and the results are presented in Figure 2. As shown in Figure 2(a), $[MoS_4]^{2-}$/CoFe-LDH was initially tested under 4% O_2, and the Hg^0 removal efficiency was approximately 90%. After 100 min of reaction, 500 ppm of SO_2 was added to the simulated flue gas. The removal efficiency was only slightly increased. SO_2 did not have an obvious poison effect on Hg^0 removal. To further indicate Hg^0 removal performance under S−Hg mixed flue gas, various concentrations of SO_2 were added to the simulated flue gas. As shown in Figure 2(b), SO_2 does not have a significant influence on the mercury adsorption capacity. Without SO_2, the mercury capacity was 1.45 mg/g. When there was 500 ppm of SO_2 in the simulated flue gas, the capacity was 1.398 mg/g. The mercury capacities were 1.31 and 1.36 mg/g under 1000 ppm of SO_2 or 2000 ppm of SO_2, respectively. Obviously, $[MoS_4]^{2-}$/CoFe-LDH can uptake Hg^0 from S−Hg mixed flue gas under low or high concentrations of SO_2.

Characterization of As-Prepared Materials. The FT-IR spectroscopy shown in Figure 3(a) verified the formation of a $[MoS_4]^{2-}$ bridged compound. In the spectrum of CoFe-LDH, a strong band appearing at 1347 cm^{-1} corresponds to the NO_3^- of the NO_3^--LDH.[29,30] This band diminished after $[MoS_4]^{2-}$ and S_4 bridged in the NO_3^--LDH materials, suggesting that NO_3^- ions were exchanged by $[MoS_4]^{2-}$ and S_4 ions. Peaks at 3377 cm^{-1} were assigned to surface molecular water. After $[MoS_4]^{2-}$ bridged into the CoFe-LDH layers, some peaks in the range of 500−550 cm^{-1} were assigned to Mo−S stretching bands. Figure 3(b) shows the XRD patterns of CoFe-LDH, S_4/CoFe-LDH, and $[MoS_4]^{2-}$/CoFe-LDH materials. The XRD patterns of S_4/CoFe-LDH were similar to that of CoFe-LDH. The basal spacing of CoFe-LDH was 0.622 nm. After $[MoS_4]^{2-}$ intercalated in CoFe-LDH, this spacing was enlarged to 0.880 nm, indicating that $[MoS_4]^{2-}$ bridged in the interlayer space.[29] Furthermore, the reflection peaks at 10−13° indicated that $[MoS_4]^{2-}$/CoFe-LDH had a layered phase.[27]

As shown in Table 1, the BET surface areas, pore volume, and pore diameter of each material were tested. CoFe-LDH material has a surface area of 41.4 m^2/g. $[MoS_4]^{2-}$/CoFe-LDH has a surface area of 112.1 m^2/g, which was three times larger than that of CoFe-LDH. The average pore diameter of $[MoS_4]^{2-}$/CoFe-LDH decreased and the pore volume increased, resulting in a large surface area. For comparison, the BET surface area of S_4/CoFe-LDH was only 21.1 m^2/g, which was smaller than that of CoFe-LDH.

Table 1. BET Surface Areas, Pore Volume, and Pore Diameter

samples	BET surface areas (m^2/g)	pore volume (m^3/g)	pore diameter (nm)
CoFe-LDH	41.432	0.238	3.551
S_4/CoFe-LDH	21.069	0.187	24.753
$[MoS_4]^{2-}$/CoFe-LDH	112.077	0.287	3.031

Furthermore, the TEM and SEM images of $[MoS_4]^{2-}$/CoFe-LDH are shown in Figure 4(a)−(f). Figure 4(a) shows the TEM image of CoFe-LDH material, which had a layered morphology. The SEM image in Figure 4(d) further indicated the layered morphology of CoFe-LDH. Figure 4(b) gives the TEM image of S_4/CoFe-LDH, and the material has a layered morphology. However, the layered sheets were not as clear as those of CoFe-LDH from the SEM image shown in Figure 4(e). Some poly sulfur stacks on the surface of LDH sheets. As shown in Figure 4(c), the composite of $[MoS_4]^{2-}$/CoFe-LDH had a layered morphology with benefits for gas molecule transfer on its surface. Figure 4(f) gives the SEM image of $[MoS_4]^{2-}$/CoFe-LDH; the layered sheets stack together and had a fluffy state when $[MoS_4]^{2-}$ was added to the CoFe-LDH materials.

Based on physical-characterization results, $[MoS_4]^{2-}$ clusters were bridged in CoFe-LDH layers using the ion-exchange method. With the addition of $[MoS_4]^{2-}$ clusters into CoFe-LDH materials, a porous structure was built which can benefit enlarging the surface area of such a composite. In addition, such

DOI: 10.1021/acs.est.7b02537
Environ. Sci. Technol. 2017, 51, 10109−10116

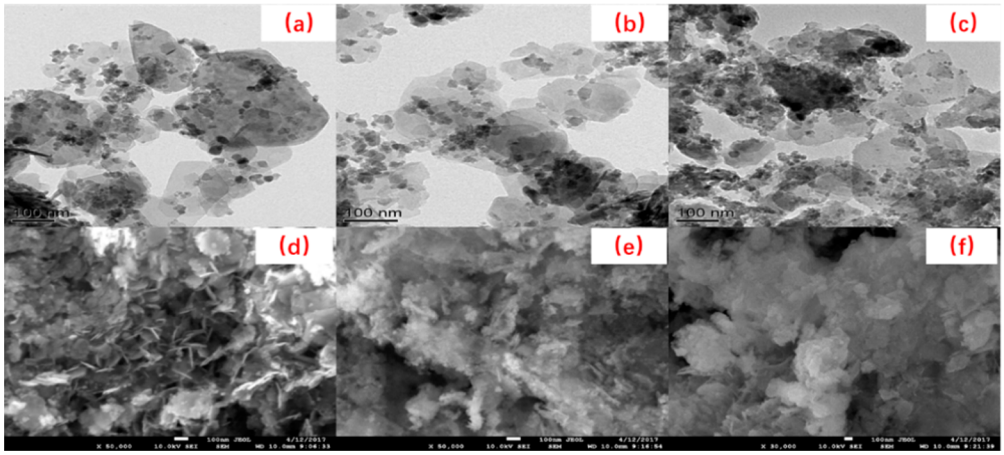

Figure 4. TEM images of (a) CoFe-LDH, (b) S_4/CoFe-LDH, and (c) $[MoS_4]^{2-}$/CoFe-LDH materials and SEM images of (d) CoFe-LDH, (e) S_4/CoFe-LDH, and (f) $[MoS_4]^{2-}$/CoFe-LDH materials.

a structure was also beneficial for Hg^0 molecule uptake on its surface.

Mechanism Study of Hg^0 Removal. The XPS analysis for the fresh samples is shown in Figure 5. As shown in Figure 5(a), for the O 1s of each sample, three peaks for CoFe-LDH, S_4/CoFe-LDH, and $[MoS_4]^{2-}$/CoFe-LDH, centered at 530.9, 531.1, and 530.0 eV, were assigned to hydroxyl oxygen.[31] For Mo 3d in Figure 5(b), the peaks at 235.1 and 232.4 eV were attributed to Mo 3d5/2 and Mo 3d3/2 XPS spectra for Mo^{6+}, respectively.[32] The peaks at 229.6 and 227.3 eV can be assigned to Mo 3d5/2 XPS spectra for Mo−S species. For S 2p in Figure 5(c), in the spectra of S_4/CoFe-LDH, two peaks at 168.6 and 164.0 eV corresponded to poly sulfur and surface sulfate, respectively.[33] The ratio of poly sulfur to surface sulfate was 62.4:37.6. The higher poly sulfur ratio indicated that S existed in the −S−S−S−S− state. Two peaks were also detected in the spectra of $[MoS_4]^{2-}$/CoFe-LDH; they were centered at similar positions and assigned to poly sulfur and surface sulfate. However, the ratio of poly sulfur to surface sulfate changed to 22.2:77.8, indicating that sulfur primarily existed in the Mo−S binding state.

After reaction under 4% O_2 and 350 $\mu g/m^3$ Hg^0 for 180 min, the spent $[MoS_4]^{2-}$/CoFe-LDH samples were analyzed by XPS. As shown in Figure 5(d), the O peak at 531.1 eV was assigned to hydroxyl oxygen. In addition, there were no other peaks detected, indicating that oxygen was not the active site for mercury adsorption. For Mo 3d in Figure 5(e), there were no obvious changes in its spectra. However, for S 2p spectra in Figure 5(f), two peaks at 168.5 and 163.1 eV were assigned to poly sulfur and sulfate, respectively. The ratio of poly sulfur was slightly increased, indicating that part of the S was combined with mercury. As shown in Figure 5(g), one peak at approximately 100.5 eV can correspond to surface HgS. Mercury primarily existed as HgS on the surface of the $[MoS_4]^{2-}$/CoFe-LDH composite.

After reaction under 4% O_2, 500 ppm of SO_2, and 350 $\mu g/m^3$ Hg^0 for 180 min, the spent $[MoS_4]^{2-}$/CoFe-LDH samples were analyzed by XPS. The oxygen was also not obviously changed in its spectra (Figure 5(h)). However, as shown in Figure 5(i), for Mo 3d, the peaks at 229.3 and 227.1 eV, which correspond to Mo−S species, were increased. This finding indicated that sulfate formed during the reaction under a SO_2 atmosphere. As shown in Figure 5(j), two peaks at 163.5 and 168.4 eV corresponded to surface sulfate and poly sulfur, respectively. After reaction, two peaks appeared at the same peak position, indicating the sulfur species did not change during the reaction. However, the mass ratio of surface sulfate increased from 65.79% to 69.24% compared to that in an atmosphere without SO_2, suggesting that some sulfate was generated during the reaction by adsorbing SO_2 from the simulated flue gas. As the Hg 4f spectra showed in Figure 5(k), there were no obvious peaks that can be detected which corresponded to surface HgS due to the high intensity of Si which centered at 102.8 eV.

A H_2-temperature-programmed reduction (H_2-TPR) measurement was performed. Figure 6(a) shows the TPR profiles of as-prepared $[MoS_4]^{2-}$/CoFe-LDH samples with S_4/CoFe-LDH and CoFe-LDH as reference samples. CoFe-LDH gave rise to three peaks that were centered at 306, 438, and 544 °C. The first peak at a temperature of 306 °C was ascribed to the reduction of Co_3O_4 to CoO.[34] A broad peak was observed at the temperature range from 375 to 600 °C, which indicates the reduction of CoO to Co, Fe_2O_3 to Fe_3O_4, and Fe_3O_4 to FeO. For the profile of S_4/CoFe-LDH, there were four peaks at 256, 322, 395, and 452 °C. However, it has a large peak centered at 395 °C. The primary reduction reaction was centered at 395 °C, indicating that poly-S_4 resulted in a reduction with a small temperature range. However, for the profile of $[MoS_4]^{2-}$/CoFe-LDH, three peaks were located at 309, 379, and 476 °C. It is difficult to define a clear boundary between each of the reduction peaks. The first temperature reduction peak (309 °C) was higher than the first peak of CoFe-LDH. The last peak was lower than that of CoFe-LDH, which indicated that $[MoS_4]^{2-}$ was beneficial for structural and thermal stability. During the reduction process, the clusters were also beneficial for electron transfers among the CoFe-LDH layers, resulting in reduction in a small range. The results suggest a strong synergistic effect between $[MoS_4]^{2-}$ clusters and CoFe-LDH, which has a beneficial influence on their adsorption performance.

Furthermore, the Hg-temperature programed desorption (Hg-TPD) method was used to detect the desorption performance. After 20 min of reaction, the spent material was passed to pure N_2 at a temperature increase from 75 to 600 °C. As shown in Figure 6(b), mercury began to be released from the surface of spent $[MoS_4]^{2-}$/CoFe-LDH at approximately 180 °C and had a maximum desorption rate at 250 °C. After 60 min of reaction, almost all surface mercury was released from the material surface. At such a desorption temperature range,

DOI: 10.1021/acs.est.7b02537
Environ. Sci. Technol. 2017, 51, 10109−10116

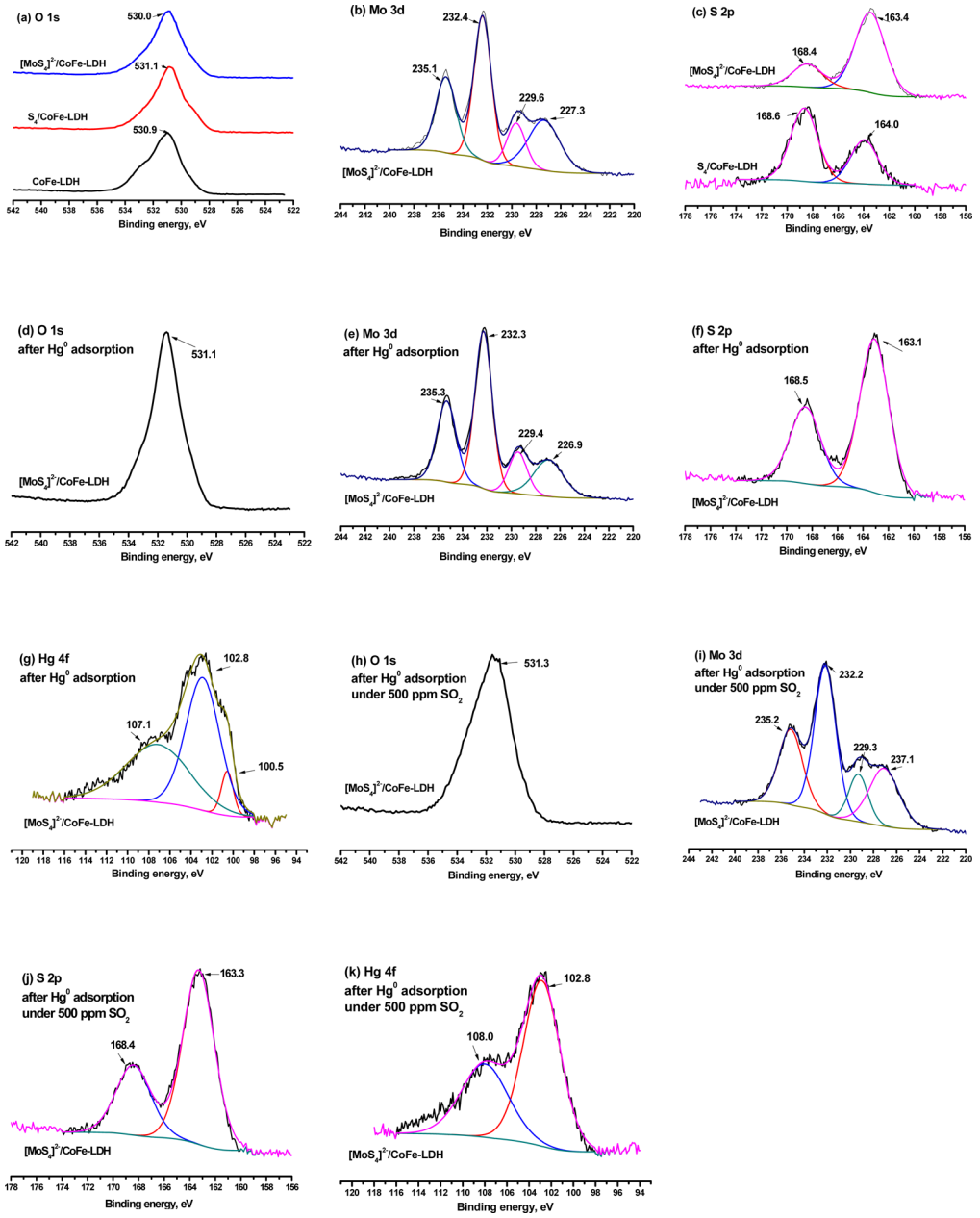

Figure 5. XPS analysis for fresh samples: (a) O 1s of CoFe-LDH, S_4/CoFe-LDH, and $[MoS_4]^{2-}$/CoFe-LDH; (b) Mo 3d of $[MoS_4]^{2-}$/CoFe-LDH; (c) S 2p of S_4/CoFe-LDH and $[MoS_4]^{2-}$/CoFe-LDH; after Hg^0 adsorption samples of $[MoS_4]^{2-}$/CoFe-LDH for (d) O 1s, (e) Mo 3d, (f) S 2p, and (g) Hg 4f; and after Hg^0 adsorption under 500 ppm of SO_2 of $[MoS_4]^{2-}$/CoFe-LDH for (h) O 1s, (i) Mo 3d, (j) S 2p, and (k) Hg 4f.

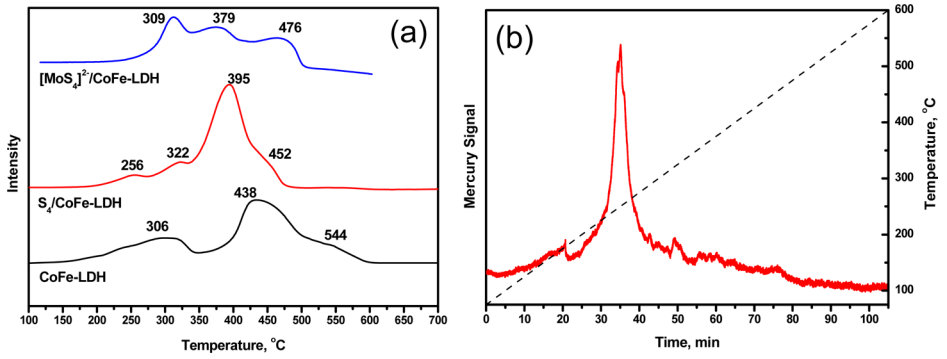

Figure 6. (a) H_2-temperature-programmed reduction (H_2-TPR) profiles of as-prepared samples and (b) Hg-temperature-programmed desorption (Hg-TPD) analysis for $[MoS_4]^{2-}$/CoFe-LDH materials.

DOI: 10.1021/acs.est.7b02537
Environ. Sci. Technol. 2017, 51, 10109−10116

mercury mainly existed in the HgS state, which was identified with the result of XPS analysis.

Based on the above discussions, gaseous mercury removal over $[MoS_4]^{2-}$/CoFe-LDH was a chemical adsorption process. As shown in Scheme 1, gaseous mercury was first adsorbed on

Scheme 1. Hg^0 Removal Mechanism over the $[MoS_4]^{2-}$/CoFe-LDH Composite

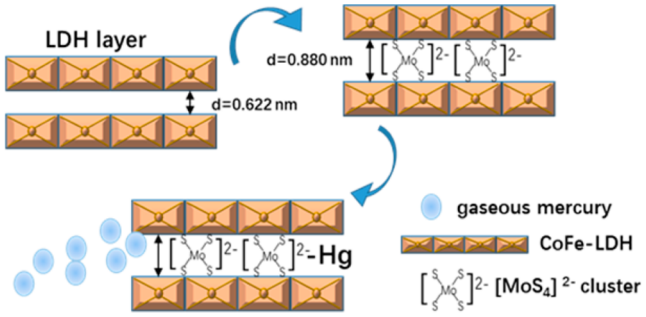

the material surface, and the special structure of CoFe-LDH was favorable for mercury physical adsorption on its surface. $[MoS_4]^{2-}$ clusters enlarged the space of CoFe-LDH layers. Gaseous elemental mercury can enter into this space and be captured by $[MoS_4]^{2-}$ clusters. Second, the adsorbed mercury bonded with S and formed HgS. The rich Mo−S network was favorable for mercury capture during this reaction.

■ ASSOCIATED CONTENT

Supporting Information

The Supporting Information is available free of charge on the ACS Publications website at DOI: 10.1021/acs.est.7b02537.

Sketch of the Hg^0 adsorption evaluation system (Figure S1), mercury adsorption breakthrough curve over $[MoS_4]^{2-}$/CoFe-LDH (Figure S2) (PDF)

■ AUTHOR INFORMATION

Corresponding Author

*Phone: +86-021-54745591. Fax: +86-54745591. E-mail: nqyan@sjtu.edu.cn.

ORCID

Wenfeng Shangguan: 0000-0001-9229-2845

Naiqiang Yan: 0000-0003-3736-4548

Notes

The authors declare no competing financial interest.

■ ACKNOWLEDGMENTS

This study was supported by the National Key R&D Program of China (2017YFC0210502), the Major State Basic Research Development Program of China (973 Program, No. 2013CB430005), and the National Natural Science Foundation of China (No. 51478261 and No. 21677096). This study was also supported by a postdoctoral innovative talent plan (No. BX201700151).

■ REFERENCES

(1) Hui, M.; Wu, Q.; Wang, S.; Liang, S.; Zhang, L.; Wang, F.; Lenzen, M.; Wang, Y.; Xu, L.; Lin, Z. Mercury flows in China and global drivers. *Environ. Sci. Technol.* **2017**, *51* (1), 222−231.

(2) Lin, Y.; Wang, S.; Wu, Q.; Larssen, T. Material flow for the intentional use of mercury in China. *Environ. Sci. Technol.* **2016**, *50* (5), 2337−2344.

(3) Pacyna, E. G.; Pacyna, J. M.; Steenhuisen, F.; Wilson, S. Global anthropogenic mercury emission inventory for 2000. *Atmos. Environ.* **2006**, *40* (22), 4048−4063.

(4) Zhao, L.; Li, C.; Zhang, X.; Zeng, G.; Zhang, J. A review on oxidation of elemental mercury from coal-fired flue gas with selective catalytic reduction catalysts. *Catal. Sci. Technol.* **2015**, *5* (7), 3459−3472.

(5) Gao, Y.; Zhang, Z.; Wu, J.; Duan, L.; Umar, A.; Sun, L.; Guo, Z.; Wang, Q. A critical review on the heterogeneous catalytic oxidation of elemental mercury in flue gases. *Environ. Sci. Technol.* **2013**, *47* (19), 10813−10823.

(6) Peng, B.; Liu, Z.; Chai, L.; Liu, H.; Yang, S.; Yang, B.; Xiang, K.; Liu, C. The effect of selenite on mercury re-emission in smelting flue gas scrubbing system. *Fuel* **2016**, *168*, 7−13.

(7) Ma, Y.; Zan, Q.; Xu, H.; Wang, W.; Yan, N.; Ma, Y.; Xu, H.; Wang, W.; Yan, N. Investigation on mercury removal method from flue gas in the presence of sulfur dioxide. *J. Hazard. Mater.* **2014**, *279*, 289−295.

(8) Suresh Kumar Reddy, K.; Al Shoaibi, A.; Srinivasakannan, C. Elemental mercury adsorption on sulfur-impregnated porous carbon − A review. *Environ. Technol.* **2014**, *35* (1), 18.

(9) Suresh Kumar Reddy, K.; Al Shoaibi, A.; Srinivasakannan, C. Elemental mercury adsorption on sulfur-impregnated porous carbon− A review. *Environ. Technol.* **2014**, *35* (1), 18−26.

(10) Vidic, R. D.; Siler, D. P. Vapor-phase elemental mercury adsorption by activated carbon impregnated with chloride and chelating agents. *Carbon* **2001**, *39* (1), 3−14.

(11) Liu, W.; Vidic, R. D.; Brown, T. D. Optimization of High Temperature Sulfur Impregnation on Activated Carbon for Permanent Sequestration of Elemental Mercury Vapors. *Environ. Sci. Technol.* **2000**, *34* (3), 483−488.

(12) Wu, J.; Zhao, Z.; Huang, T.; Sheng, P.; Zhang, J.; Tian, H.; Zhao, X.; Zhao, L.; He, P.; Ren, J. Removal of elemental mercury by Ce-Mn co-modified activated carbon catalyst. *Catal. Commun.* **2017**, *93*, 62−66.

(13) Xu, H.; Qu, Z.; Zong, C.; Huang, W.; Quan, F.; Yan, N. MnOx/Graphene for the Catalytic Oxidation and Adsorption of Elemental Mercury. *Environ. Sci. Technol.* **2015**, *49* (11), 6823.

(14) Xu, H.; Zan, Q.; Zong, C.; Quan, F.; Jian, M.; Yan, N. Catalytic oxidation and adsorption of Hg 0 over low-temperature NH 3 -SCR LaMnO 3 perovskite oxide from flue gas. *Appl. Catal., B* **2016**, *186*, 30−40.

(15) Yang, S.; Guo, Y.; Yan, N.; Wu, D.; He, H.; Xie, J.; Qu, Z.; Yang, C.; Jia, J. A novel multi-functional magnetic Fe-Ti-V spinel catalyst for elemental mercury capture and callback from flue gas. *Chem. Commun.* **2010**, *46* (44), 8377.

(16) Uddin, M. A.; Yamada, T.; Ochiai, R.; Sasaoka, E.; Wu, S. Role of SO 2 for Elemental Mercury Removal from Coal Combustion Flue Gas by Activated Carbon. *Energy Fuels* **2008**, *22* (4), 2284−2289.

(17) Reddy, G. K.; He, J.; Thiel, S. W.; Pinto, N. G.; Smirniotis, P. G. Sulfur-Tolerant Mn-Ce-Ti Sorbents for Elemental Mercury Removal from Flue Gas: Mechanistic Investigation by XPS. *J. Phys. Chem. C* **2015**, *119* (16), 8634−8644.

(18) Xu, H.; Xie, J.; Ma, Y.; Qu, Z.; Zhao, S.; Chen, W.; Huang, W.; Yan, N. The cooperation of Fe Sn in a MnO x complex sorbent used for capturing elemental mercury. *Fuel* **2015**, *140*, 803−809.

(19) Li, Y. H.; Lee, C. W.; Gullett, B. K. Importance of activated carbon's oxygen surface functional groups on elemental mercury adsorption. *Fuel* **2003**, *82* (4), 451−457.

(20) Li, H.; Zhu, L.; Wang, J.; Li, L.; Shih, K. Development of Nano-Sulfide Sorbent for Efficient Removal of Elemental Mercury from Coal Combustion Fuel Gas. *Environ. Sci. Technol.* **2016**, *50* (17), 9551.

(21) Liao, Y.; Chen, D.; Zou, S.; Xiong, S.; Xiao, X.; Dang, H.; Chen, T.; Yang, S. Recyclable Naturally Derived Magnetic Pyrrhotite for Elemental Mercury Recovery from Flue Gas. *Environ. Sci. Technol.* **2016**, *50* (19), 10562−10569.

(22) Zhao, H.; Gang, Y.; Xiang, G.; Pang, C. H.; Kingman, S. W.; Tao, W. Hg0 Capture over CoMoS/γ-Al2O3 with MoS2 Nanosheets at Low Temperatures. *Environ. Sci. Technol.* **2016**, *50* (2), 1056−1064.
(23) Oh, Y.; Morris, C. D.; Kanatzidis, M. G. Polysulfide chalcogels with ion-exchange properties and highly efficient mercury vapor sorption. *J. Am. Chem. Soc.* **2012**, *134* (35), 14604−8.
(24) Subrahmanyam, K. S.; Malliakas, C. D.; Sarma, D.; Armatas, G. S.; Wu, J.; Kanatzidis, M. G. Ion-Exchangeable Molybdenum Sulfide Porous Chalcogel: Gas Adsorption and Capture of Iodine and Mercury. *J. Am. Chem. Soc.* **2015**, *137* (43), 13943−8.
(25) Ma, S.; Chen, Q.; Li, H.; Wang, P.; Islam, S. M.; Gu, Q.; Yang, X.; Kanatzidis, M. G. Highly selective and efficient heavy metal capture with polysulfide intercalated layered double hydroxides. *J. Mater. Chem. A* **2014**, *2* (26), 10280−10289.
(26) Shami, Z.; Amininasab, S. M.; Shakeri, P. Structure-Property Relationships of Nano-Sheeted 3D Hierarchical Roughness MgAl-Layered Double Hydroxide Branched to Electrospun Porous Nanomembrane: A Superior Oil-Removing Nanofabric. *ACS Appl. Mater. Interfaces* **2016**, *8* (42), 28964−28973.
(27) Wang, Q.; O'Hare, D. Recent Advances in the Synthesis and Application of Layered Double Hydroxide (LDH) Nanosheets. *Chem. Rev.* **2012**, *112* (7), 4124−55.
(28) Ma, S.; Shim, Y.; Islam, S. M.; Subrahmanyam, K. S.; Wang, P.; Li, H.; Wang, S.; Yang, X.; Kanatzidis, M. G. Efficient Hg Vapor Capture with Polysulfide Intercalated Layered Double Hydroxides. *Chem. Mater.* **2014**, *26* (17), 5004−5011.
(29) Ma, L.; Wang, Q.; Islam, S. M.; Liu, Y.; Ma, S.; Kanatzidis, M. G. Highly Selective and Efficient Removal of Heavy Metals by Layered Double Hydroxide Intercalated with the MoS42- ion. *J. Am. Chem. Soc.* **2016**, *138* (8), 2858−2866.
(30) Ma, S.; Huang, L.; Ma, L.; Shim, Y.; Islam, S. M.; Wang, P.; Zhao, L.-D.; Wang, S.; Sun, G.; Yang, X. Efficient uranium capture by polysulfide/layered double hydroxide composites. *J. Am. Chem. Soc.* **2015**, *137* (10), 3670−3677.
(31) Deng, L.; Shi, Z.; Peng, X. Adsorption of Cr (vi) onto a magnetic CoFe 2 O 4/MgAl-LDH composite and mechanism study. *RSC Adv.* **2015**, *5* (61), 49791−49801.
(32) Zhang, Z.; Liu, B.; Wang, F.; Zheng, S. High-temperature desulfurization of hot coal gas on Mo modified Mn/KIT-1 sorbents. *Chem. Eng. J.* **2015**, *272*, 69−78.
(33) Liao, Y.; Chen, D.; Zou, S.; Xiong, S.; Xiao, X.; Dang, H.; Chen, T.; Yang, S. A recyclable naturally derived magnetic pyrrhotite for elemental mercury recovery from the flue gas. *Environ. Sci. Technol.* **2016**, *50* (19), 10562−10569.
(34) Xue, L.; Zhang, C.; He, H.; Teraoka, Y. Catalytic decomposition of N 2 O over CeO 2 promoted Co 3 O 4 spinel catalyst. *Appl. Catal., B* **2007**, *75* (3-4), 167−174.

DOI: 10.1021/acs.est.7b02537
Environ. Sci. Technol. 2017, 51, 10109−10116